River flow in the near future: a global perspective in the context of a high-emission climate change scenario

Omar V. Müller[1,2], Patrick C. McGuire[3], Pier Luigi Vidale[3], and Ed Hawkins[3]

[1]Consejo Nacional de Investigaciones Científicas y Técnicas (CONICET), Santa Fe, Argentina.
[2]Centro de Variabilidad y Cambio Climático (CEVARCAM), Facultad de Ingeniería y Ciencias Hídricas (FICH), Universidad Nacional del Litoral (UNL), Santa Fe, Argentina.
[3]Department of Meteorology, National Centre for Atmospheric Science, University of Reading, Reading, United Kingdom

Correspondence: Omar V. Müller (ovmuller@unl.edu.ar)

Abstract. There is high confidence that global warming intensifies all components of the global water cycle. Our goal is to investigate the possible effects of the global warming on river flows worldwide in the coming decades. We conducted 18 global hydrological simulations to assess how the river flows are expected to change in the near future (2015-2050) compared to the recent past (1950-2014). The simulations are forced by runoff from HighResMIP-CMIP6 GCMs, which assume a high-emission scenario for the projections. The assessment includes estimating the signal-to-noise (S/N) ratio and the time of emergence (ToE) of all the rivers in the world, with further evaluation of those presenting significant departures from their historic mean flow. Consistent with the water cycle intensification, the hydrological simulations project a clear positive global river discharge trend from ∼2000, that emerges beyond the levels of natural variability and becomes 'unfamiliar' by 2017 and 'unusual' by 2033. This climate change signal is dominated by strong increases in flows of rivers originating in central Africa, east Russia, Alaska and Greenland. African rivers project most future annual cycles above the climatological annual cycle, with the largest differences occurring during peak flows. Recent unprecedent floods in the Republic of Congo, D.R.C., Nigeria, and Chad highlight the potential catastrophic consequences of these changes in metropolitan areas. However, the positive trend of Lake Chad tributaries may aid its recovery from the strong reduction observed since the 1970s. Lastly, the projected Nile streamflow rise reinforces the need for collaboration in dam management. The simulated and observed extra release of freshwater into the Arctic Ocean produces a freshening of the ocean, potentially impacting the global ocean overturning circulation. It is concerning that several important rivers are projected to exceed their natural variability. However, the hydrological predictions assume a very high baseline emission scenario and should be interpreted as an upper limit for decision-making.

1 Introduction

Rivers play a vital role in the Earth System, being essential for the global water cycle, habitat, transport, agriculture, and energy. At the same time, under anomalous conditions, rivers may cause devastating damage through floods or by limiting navigability and water abstraction. As an integrator of the water balance over land, river flow is sensitive to changes in precipitation, evapotranspiration, and soil moisture. Shifts in regional precipitation amount, intensity, and patterns, and/or in the interplay

between soil moisture and evapotranspiration regimes, may produce anomalous river flow. The magnitude of the anomaly will
depend on the type of catchment and the intensity of the change.

There is high confidence that global warming has modified all components of the global water cycle in recent decades
(Caretta et al., 2022). The observed changes vary from regions with increased mean and extreme land precipitation to regions
with reduced precipitation, or even zones with heavier precipitation events separated by longer dry spells. Evapotranspiration
has changed in response to changes in precipitation and warmer temperatures, altering the ability of the soil to hold moisture.
Moreover, higher temperatures directly alter snow accumulation and ablation processes causing shrinking of mountain glaciers,
land ice, and snow cover. All these changes directly affect runoff generation, and thereby river flow variability, and even river
flow trends. Dai et al. (2009) reported significant (both positive and negative) trends in 55 large rivers during 1948–2012.
Alkama et al. (2011) reinforces the notion that runoff trends are a regional scale issue. They attribute these trends to precipita-
tion variability while also emphasizing the potential impact of human-induced global warming on high-latitude river discharge,
specifically through its effect on permafrost and glaciers. Similarly, Gudmundsson et al. (2021) reported heterogeneous trend
patterns across the world in low, mean, and high flow, with some rivers drying and others wetting during 1971-2010.

The continuation of global warming is expected to intensify the exchanges of water between the land, the ocean, and the
atmosphere (Alkama et al., 2013; Douville et al., 2021). In all scenarios, the CMIP6 multi-model ensemble projects an overall
increase in mean and extreme land precipitation, but with substantial variations across regions. Projected changes in evapo-
transpiration and soil moisture remain uncertain, as they are not only modulated by meteorological changes but also by plant
acclimation to higher CO_2 (Lemordant and Gentine, 2019; Oliver et al., 2022). This uncertainty extends to runoff, and by that,
to streamflow. Douville et al. (2021) conclude, with medium confidence, that global runoff will rise in the future decades but
with significant regional variations. The confidence in an overall increased runoff rises with emissions scenarios, consistent
with the strengthening of the global land precipitation.

Considering the observed and the expected changes in global runoff and knowing their strong regional variability, it is
relevant to explore how the runoff changes alter the flow of all rivers of the world. A first approach is to quantify the magnitude
of the changes in river flow (e.g., Nijssen et al. 2001; Koirala et al. 2014; Döll et al. 2018; Gudmundsson et al. 2021). But, an
extra step that enhance such standard analysis is to locally determine the signal-to-noise (S/N) ratio of any changes and estimate
the time of emergence (ToE). These concepts, initially used in the IPCC AR4 (Christensen et al., 2007), indicates where and
when a climate change signal emerges from the background natural variability, i.e., where and when the climate change might
start having larger impacts (Hawkins et al., 2020). The ToE methods are often applied to temperature (e.g., Mahlstein et al.
2011; Hawkins and Sutton 2012; Mora et al. 2013) and precipitation (e.g., Giorgi and Bi 2009; Mahlstein et al. 2012; Hawkins
et al. 2020), albeit rarely for other variables. Some exceptions are Lyu et al. (2014) who estimated the ToE for sea-level in a
global study, or Muelchi et al. (2021) who calculated the ToE for runoff in Switzerland. Given that changes in rivers due to
changing climate have potentially far reaching implications for human populations (Nijssen et al., 2001), further research about
their evolution and their ToE is expected to provide valuable information for impact and adaptation studies.

The main purpose of this paper is to provide an insight of the possible effects of global warming in a high-emission scenario
on river flows at the global scale over the next few decades. In order to fulfil this objective, we simulate rivers worldwide by

forcing a hydrological model with runoff from CMIP6 GCMs, evaluate their anomalies, and calculate their ToE. The rivers

60 of the world presenting stronger signal of climate change are further explored to infer the potential impacts of such changes. The study is organized as follows: Sect. 2 describes the used GCMs, the hydrological model, and the river flow assessment methodology; Sect. 3 examines river flow changes and their ToE with focus on the rivers of the world that are expected to change the most; and Sect. 4 presents a discussion of the results and summarizes the concluding remarks.

2 Data and methods

2.1 GCM simulations and river routing model

A set of 18 GCM simulations (see Table 1), produced within the framework of the High Resolution Model Intercomparison Project (HighResMIP v1.0) for CMIP6 (Haarsma et al., 2016), force the river routing model used to evaluate the rivers in the near future. These HighResMIP experiments were selected based on the availability of surface and subsurface runoff. The simulations include five different GCM families: CNRM-CM6 (Decharme et al., 2019; Voldoire et al., 2019), EC-Earth3P

70 (Haarsma et al., 2020), HadGEM-GC31 (Williams et al., 2018), MRI-AGCM3-2 (Mizuta et al., 2012), and NICAM16 (Kodama et al., 2021), which vary in the simulation type and the horizontal resolution. The simulation type can either be atmosphere-land (AMIP) or ocean-atmosphere-land (COUPLED). All GCMs present AMIP simulations, but just CNRM-CM6, EC-Earth3P, and HadGEM-GC31 have COUPLED simulations. In addition, all GCMs produced a low- and a high-resolution simulation, except for the HadGEM-GC31 family that also provides at intermediate-resolution. To conciliate the variety of grid topologies used

75 by the different GCMs (rectilinear, reduced gaussian, icosahedral, etc), we provide the atmospheric horizontal resolution at $50°N$, which ranges from 25 km to 134 km for the set of simulations. For COUPLED simulations we also provide the ocean resolution, which varies from 1 deg for low-resolution to 0.25 deg for high-resolution simulations. Note that there is only one member per resolution and simulation type, which may makes the projections susceptible to the internal variability. However, in Appendix A we show that the inter-model variability is much larger than the internal variability, which suggests strong

80 robustness of the used set of simulations.

The total runoff (surface and subsurface) produced by each GCM simulation is used to force a river routing model, which is a standalone version of the Total Runoff Integrating Pathways (TRIP) model (a detailed model description is given in Müller et al. 2021a). The routing model collects the runoff from each grid cell and drives it through the river network estimating the river storage and outflow of each grid cell of the network. The model does not gain or lose water, thus, the simulated outflow

85 can be directly associated to the GCM forcing the simulation. The simulations are run globally (excluding Antarctica) at a common resolution of 0.25 °, using nearest-neighbour to regrid the runoff from the original GCM resolutions to the target grid. The river network at quarter degree is based on the flow direction of the Dominant River Tracing dataset (Wu et al., 2011, 2012).

The hydrological simulations span from 1950 to 2050 at monthly time-scale, considering 1950-2014 as the present clima-

90 tology (hereinafter PRESENT), and 2015-2050 as the near future (hereinafter FUTURE). Note that the projections in HighResMIP consider a scenario as close to CMIP5 RCP8.5 as possible within CMIP6 (Haarsma et al., 2016), i.e., the hydrological

Table 1. GCM simulations.

GCM	Simulation type AMIP, COUPLED	Atmosphere horizontal resolution at $50°$ [km]	Ocean resolution for COUPLED [deg]	Warming [$°$C] AMIP, COUPLED
CNRM-CM6-1	yes, yes	100	1.00	1.2, 1.4
CNRM-CM6-1-HR	yes, yes	35	0.25	1.2, 1.3
EC-Earth3P	yes, yes	80	1.00	1.1, 1.4
EC-Earth3P-HR	yes, yes	39	0.25	1.1, 1.3
HadGEM-GC31-L*	yes, yes	134	1.00	1.2, 2.0
HadGEM-GC31-MM	yes, yes	60	0.25	1.2, 1.7
HadGEM-GC31-HM	yes, yes	25	0.25	1.2, 1.8
MRI-AGCM3-2-H	yes, no	60	—-	1.2, —-
MRI-AGCM3-2-S	yes, no	20	—-	1.2, —-
NICAM16-7S	yes, no	56	—-	1.1, —-
NICAM16-8S	yes, no	28	—-	1.1, —-

*=M for AMIP (HadGEM-GC31-LM) and

*=L for COUPLED (HadGEM-GC31-LL)

predictions are appraised in the context of a high emission scenario. Table 1 indicates the change in global temperature between FUTURE and PRESENT as an indicator of the assumed scenario impact on the projections. AMIP projections present a warming of $\sim$1.2 $°$C, while COUPLED projections present a change ranging from 1.3 $°$C to 2 $°$C. Although such changes

95 may seem large for short-term climate predictions (36 years), they are likely to occur in the long-term.

2.2 Assessment methodology

To understand the expected changes in rivers in the next decades, we perform a three-steps analysis. First, we identify the main differences between FUTURE vs PRESENT in key hydrological variables. Second, we estimate the ToE of global river discharge. Lastly, we focus the evaluation of river flow on potentially hazardous rivers due to the projected significant departures

100 from their historic mean flow.

In the comparison of FUTURE vs PRESENT we assess the expected anomalies of land precipitation and total runoff in the near future (2015-2050) with respect to the recent past (1950-2014), used as reference climatology. A particular interest is given to the level of agreement among GCMs in such changes, which ensure robustness to the climate change signal (if any). Then, we centre the analysis in streamflow to understand how the anomalies in runoff end up affecting the different rivers of

105 the world.

The river discharge S/N ratio and ToE is calculated following the approach proposed by Hawkins and Sutton (2012). The goal of the method is to decouple the climate change signal (S) from the natural variability (the noise N). In our work, the method is applied to the river discharge annual anomaly (Q) of each simulation. PRESENT is used as the base-period to calculate the anomalies in the entire period (1950-2050).

At the global scale, the signal $S_G(t)$ is a low-pass filtered version of the original Q_G time-series. The filter is based on the convolution of a scaled window with the signal, and has a smoothing effect of the inter-annual variability. On the other hand, the noise is a fixed value calculated as $N_G = \sigma(Q_G(t) - S_G(t))$ over the base-period, where σ is the standard deviation. At the local scale (grid box), the signal is a linear regression of the local river flow annual anomaly $Q_L(t)$ onto the global signal $S_G(t)$, that is, $S_L(t) = mS_G(t) + b$, where m and b are the regression coefficients (slope and intercept respectively). The local noise is then estimated similarly to the global case as $N_L = \sigma(Q_L(t) - S_L(t))$ over the base-period.

Both scales (global and local) use the corresponding noise as a threshold to determine the year in which the signal of climate change emerges from the natural variability. Following the terminology used by Frame et al. (2017) and Hawkins et al. (2020), the year t in which $|S(t)| > N$ is described as ToE to 'unfamiliar' climate, while the year in which $|S(t)| > 2N$ as ToE to 'unusual' climate conditions. Conversely, $|S(t)| < N$ means that the projections of river flow remain in the range of its historical variability.

The previous analysis allows the identification of the rivers of the world whose predictions suggest a shift from their known climate to an unfamiliar or even to an unusual climate. The changes on this set of rivers is individually assessed to determine when the shift is expected to occur, how it alters the annual cycle dynamics, and its potential impact on metropolitan areas, dams management, and ocean circulation.

3 Results

3.1 Changes in the land water budget

Precipitation, evapotranspiration, and runoff are the main components of the long-term land water budget and thereby, the key hydrological variables to understand long-term changes in rivers. Figure 1 compares how the global mean values of these variables change in the projections with respect to the climatology. Notably, all the models agree in the prediction of wetter conditions for the next decades independently of the type of simulation (AMIP or COUPLED) and the model's resolution. However, the positive changes in the projections of precipitation and runoff tend to be stronger for the the COUPLED simulations, likely due to the higher level of global warming they simulate for the FUTURE period (see Table 1). On the other hand, for each GCM family, increasing the resolution results in higher values for both the PRESENT and FUTURE periods. That is because high-resolution models enhance ocean-land moisture transport, producing more realistic mesoscale circulation patterns and synoptic systems (Vannière et al., 2019; Müller et al., 2021b). Moreover, the better-resolved orography at high-resolution favours the organization of convective precipitation and improves the representation of orographic jets producing more orographic precipitation, and thereby more runoff in the headwaters (Vellinga et al., 2016; de Souza Custodio et al., 2017; Vannière et al., 2019; Müller et al., 2021a). The differences that arise with resolution and the level of warming produces
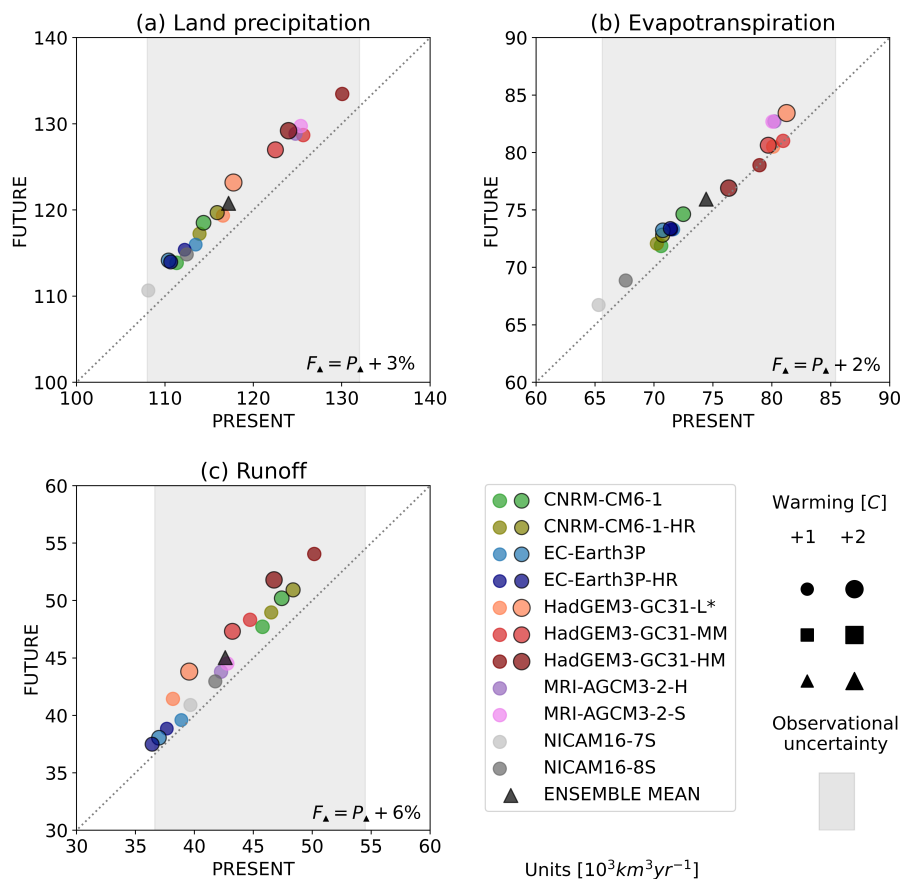
Figure 1. Scatterplots of the global land surface water budget components: (a) precipitation, (b) evapotranspiration, and (c) runoff comparing PRESENT mean vs FUTURE mean of each GCM simulation. Circles are for AMIP type simulations, squares are for COUPLED simulations, and triangles represent the ensemble mean based on the 18 simulations. The markers' size is proportional to the degree of warming of each simulation (see values in Table 1). The identity line is plotted in dotted grey. The legend in the bottom right corner of each scatterplot indicates the percentage change between FUTURE and PRESENT of the ensemble mean ($F_{\blacktriangle}$ and $P_{\blacktriangle}$ respectively). The * in the legend means M for AMIP (HadGEM3-GC31-LM) and L for COUPLED (HadGEM3-GC31-LL). The grey bands show the observational uncertainty considering a large number of observation-based estimations including: IPCC AR6 (Caretta et al., 2022), Rodell et al. (2015), Trenberth et al. (2007), ERA5 (Hersbach et al., 2020), CRU TS4.05 (Harris et al., 2020), WFDEI (Weedon et al., 2018), CPC (Chen et al., 2008), FLUXCOM (Jung et al., 2019), Dai et al. (2009), Clark et al. (2015), Müller et al. (2021a), and GLOFAS (Harrigan et al., 2020). Units are in $10^3 \text{km}^3\text{yr}^{-1}$.

a spread in the global mean values of the various GCMs. Even so, it is noteworthy that the values for all GCMs remain in the range of the observational uncertainty for the three variables.

140   Despite the global land precipitation increases by $3.6 \times 10^3 \text{ km}^3\text{yr}^{-1}$ in the ensemble mean, which represents just 3 % more precipitation, a large fraction of the extra water ends up in runoff, which is augmented by $2.4 \times 10^3 \text{ km}^3\text{yr}^{-1}$, representing a positive change of 6 % in the global average. The remaining extra precipitation is returned to the atmosphere through
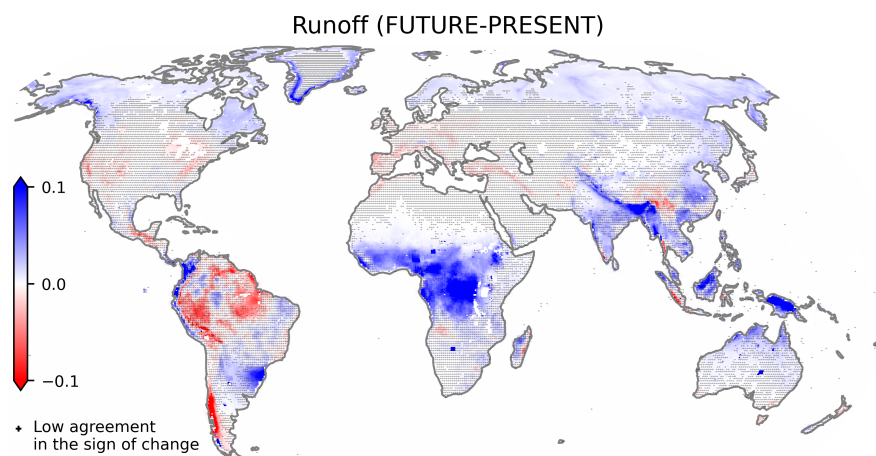
Figure 2. Multi-model ensemble mean differences in runoff [$10^3 \text{km}^3 \text{yr}^{-1}$] between FUTURE (2015-2050) and PRESENT (1950-2014). The crosses indicate that at least 3 out of 18 GCMs disagree in the sign of change.

evapotranspiration, which rises by 2 % in the ensemble mean. The global rise of land precipitation and evapotranspiration is

145 mainly explained by two factors that have a general consensus of most GCMs: a strengthening of the ITCZ and an overall wettening in the northern high-latitudes (a discussion about such phenomena is given in Appendix B).

Positive anomalies in precipitation are amplified in runoff (in terms of percentage change) when the extra water either falls over wet regions, where there is no more room for evapotranspiration or, over mountainous areas, where horizontal fluxes prevail (Müller et al., 2021a). Figure 2 shows that positive and negative changes in runoff are unevenly distributed in the world.

150 Central Africa is the most extensive region with strong wetter conditions, but also more runoff is predicted for southeast South America, India, the Maritime Continent, and the windward side of orographic barriers like Tropical Andes, Alaska Range, and the Himalayas. On the other hand, the main reductions of runoff are projected in parts of the Amazon Forest and southern Chile. There is agreement among most models on the regions presenting notable changes (either positive or negative), but also about the slight increase of runoff in the northern high latitudes, which is related to the strong signal of warming projected for

155 that area (see Fig. B1c and its description in Appendix B).

The predicted global enhancement in runoff has direct effect on river flow. Figure 3a presents the percentage change in river discharge between FUTURE and PRESENT for the catchments of the world, while Fig. 3b depicts similar information but detailed for all rivers tributaries. Consistently with the analysis of runoff, the stronger positive changes appear in African, Australian, and Boreal rivers. In Africa, many important rivers increase the mean discharge by more than 20 %, including the

160 three major rivers: Congo (+20 %), Nile (23 %), and Niger (26 %), but also Okavango (+21 %), Volta (+33 %), and rivers feeding Lake Chad, whose catchment presents the largest percentage increment (+49 %). In Australia, the major river, Murray, is augmented by 14 % while other small rivers in northern Australia (Victoria, Ord, Fitzroy) and those discharging into the Lake Eyre (Cooper, Warburton, among others) increase their flow by more than 35 %. In the boreal zone, almost all rivers simulate
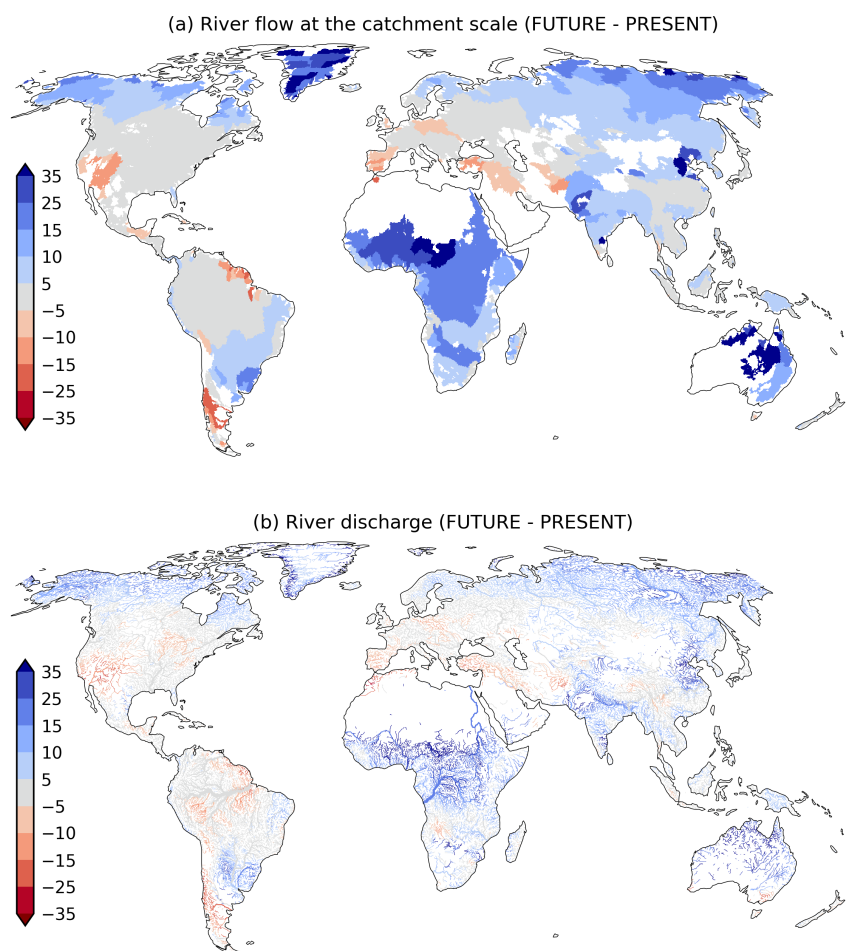
(a) River flow at the catchment scale (FUTURE - PRESENT)

(b) River discharge (FUTURE - PRESENT)

Figure 3. Multi-model ensemble mean differences in river flow between FUTURE (2015-2050) and PRESENT (1950-2014) presented as (a) the average difference at the catchment scale (i.e., the difference calculated at the river mouth of each catchment) and as (b) the difference for each channel of the river network. Rivers with little climatological flow ($< 100\,\mathrm{m^3 s^{-1}}$ at the river mouth for the top panel and $< 5\,\mathrm{m^3 s^{-1}}$ in the river channel for the bottom panel) are masked out in the maps. Units are in %.

more drainage of freshwater into the Arctic Ocean, being those located in east Russia (e.g., Lena, Yana, Kolima), and Alaska
165 (e.g., Yukon) the rivers with at least 10 % more freshwater. In South America, just the Uruguay river presents a significant rise of discharge (15 %). On the other hand, a few small rivers in the world present reduced flow for the FUTURE. For instance, rivers originating in Southern Andes (e.g., Maipo, Maule, Limay, Negro, Chubut) and Colorado in the USA decrease their flows by ∼15 %, while most rivers of the Iberian Peninsula project a decay of about ∼10 %. Interestingly several southern tributaries of Amazon present dry anomalies, but they are not sufficient to significantly alter the downstream discharge into the Atlantic
170 Ocean. In summary, a 6 % extra global runoff in the near future may seem irrelevant, but the changes are heterogeneously

distributed throughout the globe, with many important rivers changing their mean flow by more than 15 %, which suggests a clear signal of climate change.

3.2 Time of emergence

Under the imposed high-emission scenario, all GCMs project a global rise of river discharge for the next decades, and there is an
175 overall consensus among models on where the changes of river flow are likely to occur. However, there is an important spread in the magnitude of the change. Figure 4a presents the trends of global river discharge anomalies for each model. The differences among models get amplified over time and are more noticeable in COUPLED models, i.e., the stronger signal of change are simulated by the GCMs with higher warming (see Table 1). The ensemble mean global river discharge for PRESENT is $42.6 \times 10^3 \mathrm{km}^3 \mathrm{yr}^{-1}$, while the anomalies by 2050 are in the range $[0, 4.9] \times 10^3 \mathrm{km}^3 \mathrm{yr}^{-1}$ for AMIP and $[0.4, 8.1] \times 10^3 \mathrm{km}^3 \mathrm{yr}^{-1}$
180 for COUPLED. These anomalies represent a positive change of up to 11.5 % for AMIP and up to 19.0 % for COUPLED by the end of the projected period.

But, are these anomalies within the natural variability range? Figure 4b presents the ToE estimation for the ensemble mean. As for individual models, the ensemble mean presents a steady-state until about the year 2000, and a strong positive trend thenceforth. The anomalies remain within the natural variability range ($\pm N$), i.e. within the familiar climate conditions, until
185 the year 2017. From there on, the global river discharge enters in an unfamiliar climate until 2033, when it shifts to unusual climate condition.

The emergence of global river discharge can have severe implications for specific rivers around the world, such as an increased frequency of floods. Figure 5 displays the ensemble mean spatial distribution of the signal-to-noise ratio (S/N) by the year 2050, when the global signal is maximum (Figure 4b). The pattern reveals that the majority of rivers worldwide will
190 remain in a range of natural variability in the coming decades ($|S/N| < 1$). However, most changes arise in high-latitude and tropical areas where $|S/N| > 0.3$. The high-latitude changes can be attributed to polar amplification, while the tropical changes are likely due to a shift to intense precipitation in the ITCZ (see discussion in appendix B), which is accurately simulated only at resolutions finer than 20 km. In this sense, the river network may act as a strong filter, partly compensating for precipitation errors. Within high-latitude and tropical areas, rivers originating in central Africa, east Russia, Alaska, and Greenland present
195 signals of climate change ($|S/N| > 1$). Figure 6a shows that the main courses of Congo, Nile, Niger, and Chad present a ToE from familiar to unfamiliar climate during the years 2015-2025, while Yukon and Lena after 2030. Moreover, the projections of river flow in lower Congo, Oubangui (Congo's north tributary), Chari (primary tributary of Lake Chad), and Main Nile indicate a shift to unusual wetter climate condition during the 2030s (Fig. 6b). Similarly, the flow of rivers discharging in the Greenland coasts are projected to move to unusual climate in the next decade.

200 ### 3.2.1 Rivers susceptible to strong changes

The global evaluation of the signal-to-noise ratio and the time of emergence reveals that the stronger changes are projected for rivers in Africa and some rivers discharging in the Arctic Ocean. Here, we focus the analysis on those rivers for which, in light of the projections, the signal of climate change of mean flow emerges from its familiar climatology. Figure 7 shows the
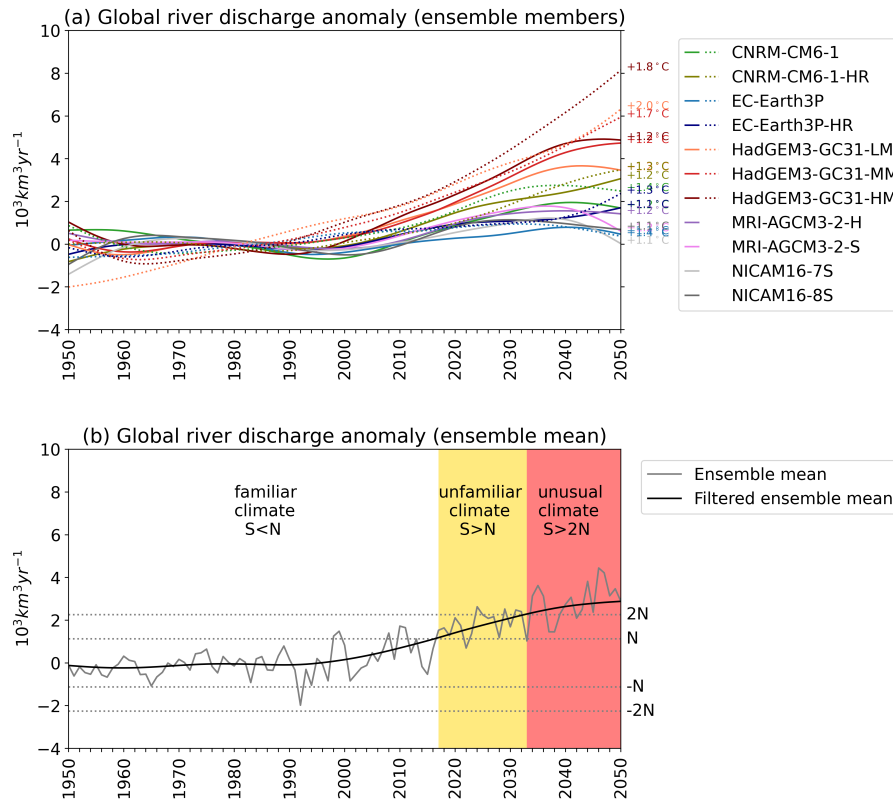
Figure 4. (a) Temporal evolution of global river discharge anomalies smoothed with a low-pass filter for each ensemble member. Solid lines are for AMIP and dashed for COUPLED simulations. Numbers on the right side indicates the average warming in the FUTURE period. (b) As (a) but for the ensemble mean in black, and the annual anomalies in grey. Dashed lines are thresholds to identify the year when the signal of climate change emerge from the natural variability (N) to unfamiliar (yellow) or unusual (red) climate conditions. In all cases the anomalies are calculated as the departure from the mean of the PRESENT period (1950-2014).

streamflow evolution from 1950 to 2050 and the annual cycles of four rivers in Africa (Congo, Niger, Chari, Nile), two rivers

205   discharging in the Arctic Ocean (Yukon and Lena), and the integration of all Greenland's rivers at their mouths. The former four are evaluated at locations where the main channels flow near important metropolises to understand the potential risk for human settlements, while the latter are evaluated at the river mouth to infer the possible effects of the discharge changes in the Arctic circulation.

     Kinshasa-Brazzaville is the third most populous metropolitan area in Africa, with the special feature of being composed by

210   two capitals separated by the Congo river near its river mouth. Kinshasa is the capital of Democratic Republic of Congo, has an estimated population of 18 million inhabitants and expands over the southern bank of the river. Brazzaville is the capital of Congo Republic, it has about 2 million inhabitants and it covers the northern side of the river. On the other hand, the Congo River has the second largest discharge of all rivers in the world. The Congo streamflow at Kinshasa-Brazzaville presents a
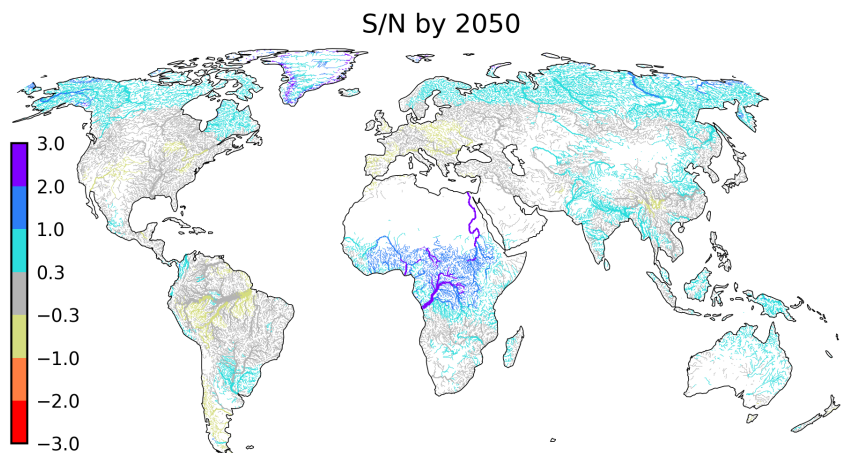
S/N by 2050

Figure 5. (a) Global map of signal-to-noise ratio of river flow by 2050. The ratio is the ensemble mean of the signal-to-noise ratio of each simulation. Rivers with little climatological flow (< 5 m^{3}s^{-1}) are masked out.

steady evolution during the past century that changes to a positive trend at the beginning of the current century (Fig. 7a). The
215 simulated streamflow rise exceeds the upper threshold of the familiar climate by the year 2018, and it drifts from unfamiliar to unusual climate by 2036 (see Fig. 7a). Interestingly, most annual cycles in the FUTURE period (2015-2050) are above the mean annual cycle of the PRESENT period (1950-2014). These differences are amplified for the two peaks in December and May, which could be up to ∼50 % higher than the climatological peaks.

The Niger is the main river of west Africa. Asaba and Onitsha are important cities that extends along the western and eastern
220 banks (respectively) of the Niger just before its delta. The port in Onitsha converted the city into a budding commercial centre with the largest market in west Africa in terms of volume of goods. The exponential commercial growth of Onitsha, together with the lack of an urban development plan, favoured the building of illegal structures especially on waterways, which may have serious consequences when Niger river overflows its banks (Obi-Ani and Isiani, 2020). Similar to the Congo river case, the Niger at Asaba-Onitsha presents no trend until ∼2000, when the streamflow starts to quickly rise, emerging from the
225 natural variability range by the year 2017 (Fig. 7b). The ensemble mean projection simulates a Niger streamflow remaining in unfamiliar climate conditions until 2036, when it shifts to unusual climate. Unlike projections for Congo, the signal of climate change stabilize close to $2N$ in the last 15 years of simulation. The Niger has a marked annual cycle, typical of a monsoon climate, with maximum in boreal autumn and minimum in boreal spring. According to the simulations, the amplitude of this annual cycle will be exacerbated due to a strong increase of flow during the wet season.
230 N'Djamena is the capital, the largest city, and the economic centre of Chad. It is placed at the confluence of Logone river into the Chari river, which flows downstream into Lake Chad. Figure 7c reveals a positive trend from the 1990s onwards combined with an increased interannual variability. The ensemble mean signal emerges from the familiar climate to unfamiliar climate by 2015, and continues rising until 2031, when the streamflow enters in unknown climate for the last two decades of simulation.
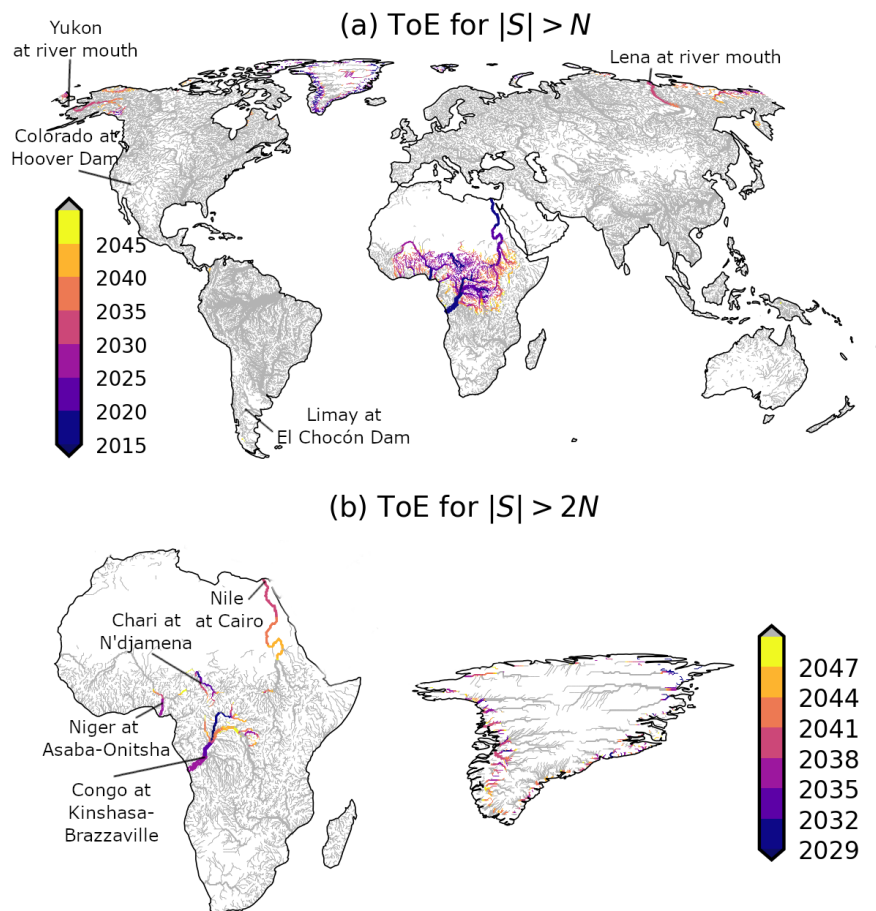
Figure 6. (a) Global map of ToE for river flow signal >1 or <-1. (b) Africa and Greenland maps of ToE for river flow signal >2 or <-2. Rivers that remain within the range of natural variability $[-N, N]$ until the end of the simulation are shown in grey. Rivers with little climatological flow ($< 5 \, \mathrm{m^3 s^{-1}}$) are masked out. Black lines and labels highlight places that are further analysed in Sect. 3.2.1.

The Chari river annual cycle is also modulated by the West African monsoon system with peaks in boreal autumn and little
235   flow in boreal spring. The projections simulate a notable increase of peaks that could almost duplicate the climatological flows.

The Nile river crosses Cairo, the ancient capital of Egypt, just behind its large delta, which discharges freshwater into the
Mediterranean Sea. Greater Cairo is the second largest metropolitan area in Africa with an estimated population of more than
20 million inhabitants. The river is used to irrigate farms, to support water consumption, and as a trade route. Under normal
conditions, the flooding season is considered a symbol of fertility as the flow brings nutrients to the river banks favouring
240   the subsequent planting and harvesting. However, the river banks are washed away during extreme floods causing negative
impacts. Figure 7d shows a positive gradient in Nile streamflow at Cairo since ~2000, with the smoothed time-series shifting
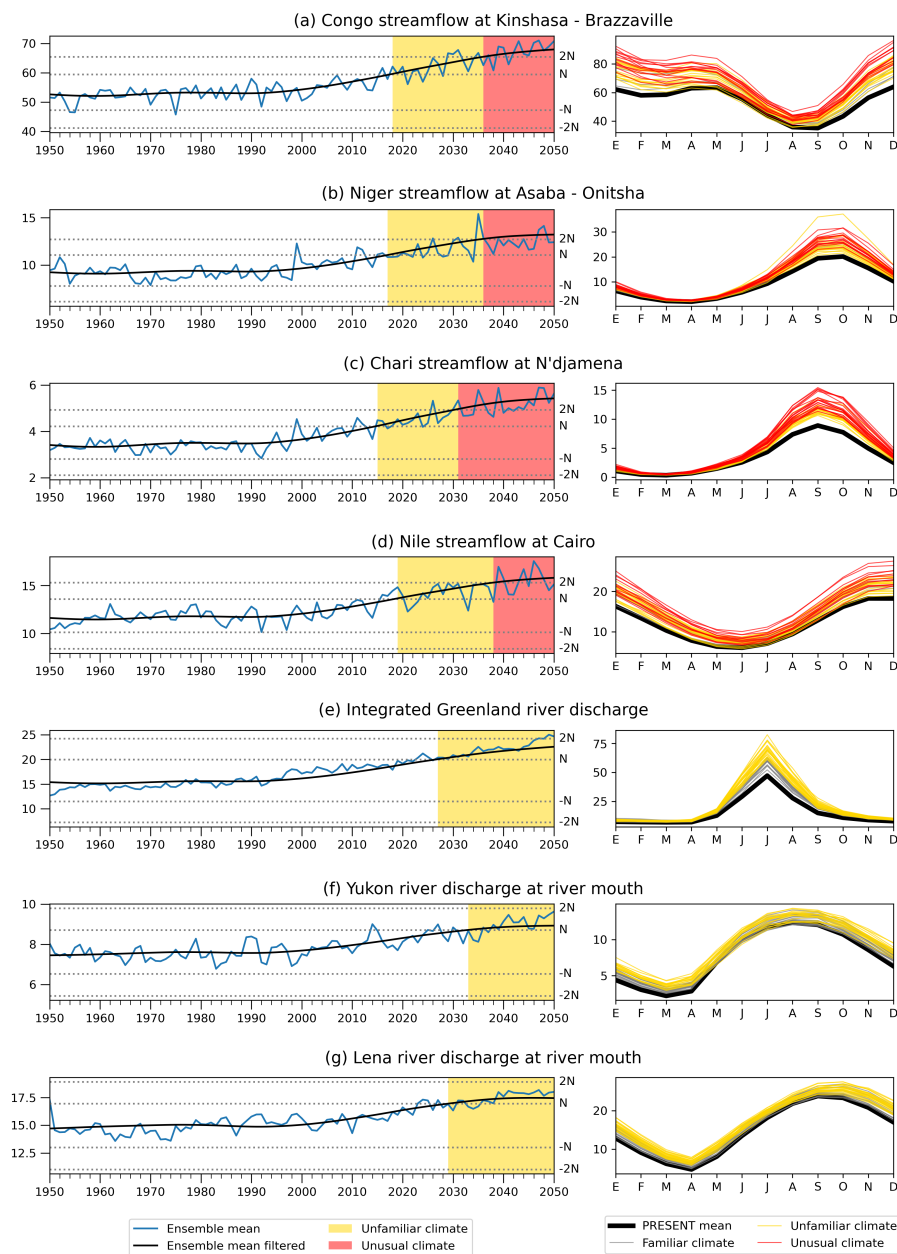
Figure 7. Temporal evolution (left) and annual cycles (right) of river flow for different rivers of the world: (a) Congo at Kinshasa - Brazzaville, (b) Nile at Cairo, (c) Niger at Asaba - Onitsha, (d) Chari at N'Djamena, (e) integration of Greenland's rivers at their mouths, (f) Lena at river mouth, and (g) Yukon at river mouth. Dashed lines (in left panels) are thresholds to identify the year when the signal of climate change emerge from the natural variability (N) to unfamiliar (yellow) or unusual (red) climate conditions. Units are in $10^3 \mathrm{m}^3 \mathrm{s}^{-1}$.
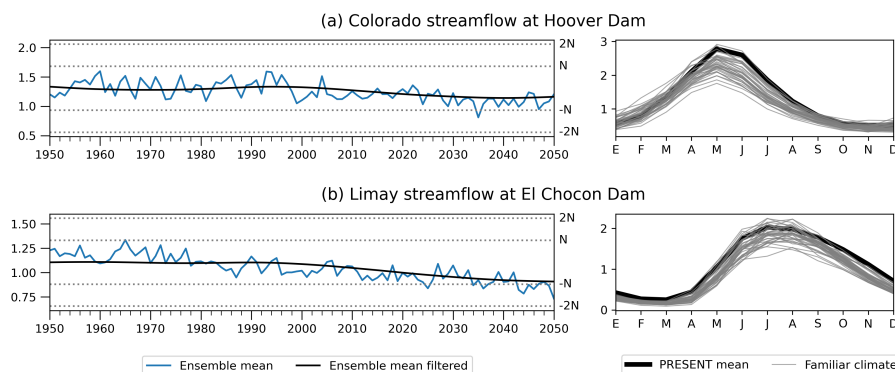
Figure 8. As in Fig. 7 for: (a) Colorado at Hoover Dam and (b) Limay at El Chocón Dam.

to unfamiliar climate by 2019, and to unknown climate conditions by 2038. The future annual cycles present positive anomalies in all seasons that become stronger for months of high flows.

The Arctic Ocean plays two roles in the global ocean circulation: it provides a pathway to connect the Pacific and the Atlantic

245 oceans; and it receives Atlantic inflow, cools the water, and returns it to the Atlantic (Rudels and Friedrich, 2000). Rivers discharging in central and northern Greenland, Yukon and Mackenzie in North America, and Ob, Yenisey, and Lena in Russia are the major tributaries of the Arctic Ocean. They all present positive anomalies for the FUTURE period (see Figs. 3 and 5). However, Greenland rivers, Yukon and Lena, which together contribute ∼23 % of the Arctic inflow, are the ones that emerge to unfamiliar condition in the near future (by 2027, 2033, and 2029 respectively) (Fig. 7e-g). The simulated annual cycles for

250 the FUTURE period of the integrated Greenland rivers present a strong enhancement of the peak in boreal summer. Instead, Yukon and Lena annual cycles show a systematic increase of flow throughout the year. However, the simulated cycles of these two rivers do not properly follow the well known dynamic of boreal rivers, which typically present little flow during winter, followed by a sharp rise of flow in late spring related to snow melt that continues during summer. The GCMs simplification of snow processes may be hindering the generation of runoff in the correct time of the year, and thereby, the real river dynamics.

255 Although positive river flow trends dominate the projections, there are some rivers of the world where models project drier conditions for the future. Figure 8 presents the cases of Colorado at Hoover Dam (the largest dam in USA) and Limay at El Chocón Dam (the fourth largest Argentinian dam). In both cases, the dry anomalies that average ∼-15 % are not strong enough to emerge from the natural variability range before 2050, but this is likely to occur in Limay in the second half of the century if its signal strengthens in the long-term ($S/N = -0.9$ in 2050). Colorado and Limay are snow-fed rivers extended

260 over arid to semi-arid regions. The streamflow decline results from a combination of reduced precipitation with increased evapotranspiration (see Fig. B1), which produces snow loss in the headwaters (Hoerling et al., 2019; Milly and Dunne, 2020).

14

4   Discussion and conclusions

We conducted 18 quarter degree global hydrological simulations for the period 1950-2050 forced by runoff from a variety of HighResMIP-CMIP6 GCMs, which assume a high-emission scenario for the projections. The simulations were used to assess
265   how the river flow is expected to change until mid-century at the global scale. The assessment included a direct comparison of key hydrological variables, and the estimation of the signal-to-noise ratio and the ToE to determine for which rivers of the world and when the climate change signal will emerge from the natural variability. Lastly, we focused the ToE analysis in a subset of rivers that, under a high-emission scenario, would face unfamiliar or even unusual climate in the coming decades.

In agreement with the IPCC AR6 (Douville et al., 2021; Caretta et al., 2022) the GCMs present a general intensification of
270   the global land water budget components for the FUTURE period. Independently of the type of simulation and the model's resolution, the GCMs systematically predict more land precipitation (+3 %), evapotranspiration (+2 %), and runoff (+6 %). The enhanced runoff is mainly supported by strong positive anomalies (>+20 %) in central Africa and slight wet anomalies in the northern high latitudes, which are partially compensated by dry anomalies in parts of South America. Beyond the large regional variations in runoff, there is strong consensus among models of which catchments are likely to present positive changes in the
275   near future (Congo, Niger, Nile, Lake Chad, Lena, Indigirka, Kolima, and Yukon). On the other hand, the models agree on negative anomalies for some rivers of the world with little flow. For instance, rivers in Patagonia (e.g., Maipo, Negro, Chubut), some tributaries of Amazon (Ukayali and Xingu), most rivers in the Iberian Peninunsula, and Colorado river in North America.

Consistently with the wettening of the global land water budget, most models project a clear positive global river discharge trend from ~2000. The signal of the ensemble mean emerges to unfamiliar climate conditions by 2017 and to unusual climate
280   conditions by 2033. Nonetheless, there is a large spread in the magnitude of the climate change signal among models, with anomalies ranging from almost no change to +19 % by 2050. The global climate change signal is supported by strong increases in mean flows of rivers originating in central Africa, east Russia, Alaska, and Greenland. In particular, the main courses of Congo, Nile, Niger, and Chad present the soonest emergence to unfamiliar climate by 2015-2025 and to unusual climate after 2030, while Yukon, Lena, and Greenland rivers also contribute to the global change entering in unfamiliar climate by ~2030.

285   It can be argued that the ensemble mean climate change signal is strongly influenced by the high-resolution versions of GCMs, which simulate greater anomalies, and thereby, sooner ToE. This is particularly true for HadGEM3-GC31, the GCM with the highest anomalies in Africa (not shown). However, Müller et al. (2021b) provide robust evidence that high-resolution GCMs notably enhance the representation of land-atmosphere interactions in Africa through improved large-scale circulation and better-resolved local processes. Moreover, Müller et al. (2021a) showed that high-resolution HadGEM3-GC31 simulations
290   notably improves the performance in mountainous regions due to the finer definition of the orography, which favours the development of orographic precipitation and more runoff, matching better with river flow observations. While uncertainty in future projections is unavoidable, these studies suggest that the GCMs projecting stronger changes for the FUTURE are those that provide the most reliable simulations for the PRESENT period.

The specific evaluation done for African rivers flowing along important cities (Congo at Kinshasa-Brazzaville, Niger at
295   Asaba-Onithsha, Chari at N'Djamena, and Nile at Cairo) revealed two common features in the four cases. First, they show a

15

pronounced signal of change in streamflow, which emerges from the background natural variability to unfamiliar conditions by ~2018, and to unusual conditions between 2031 and 2038. Second, most projected annual cycles are above the mean annual cycle of the base period, but most importantly, the amplitude of the cycles are intensified, being the annual highs the months with largest differences with respect to the historical values. The peaks are expected to rise by ~30 % on average with some

300 years augmenting above 50 %.

Such magnitude of changes for the FUTURE period (2015-2050) may produce severe floods with catastrophic consequences in metropolitan areas. Indeed, the Congo River has suffered frequent floods recently (e.g., the severe floods from October 2019 to January 2020 reported in UNOCHA 2021) affecting at least 100,000 people per year since 2015 in Republic of Congo and Democratic Republic of Congo (Ritchie and Roser, 2014). Nigeria suffered an unprecedented flood in 2012 with 7,000,000

305 people affected and 363 reported deaths (Amangabara and Obenade, 2015), but also flooding events in 2018, 2020 (Ritchie and Roser, 2014), and 2022. IFRC (2022) reported at least 2,800,0000 people affected and at least 603 lives lost in the 2022 flood, being the near delta states the most affected. Similarly, Logone and Chari overflowed their banks, hitting N'Djamena in 2012 and 2022 (UNITAR, 2012; UNOCHA, 2022; Ritchie and Roser, 2014). However, the positive trend of Lake Chad tributaries is not necessarily bad news for the region. It is well known that Lake Chad, which provides food and water to 50,000,000 people,

310 has shrunk up to 90% of its area since the 1970s (Gao et al., 2011). In agreement with the simulations, recent observation-based research has reported a recovery of the Lake Chad surface water extent and volume since 2000's (Pham-Duc et al., 2020), which brings hope to the surrounding growing communities. Lastly, the relationship between Nile flow and flooding events in Cairo is not straightforward given the strong regulation of river dynamics with dams. Thus, the projected increase in river flow may have important implications for dam management strategies, reinforcing the need for consensus and cooperation over Nile

315 waters (Conway, 2017).

The results of Yukon and Lena discharge into the Arctic Ocean also revealed two common patterns. Their projections shift from familiar to unfamiliar climate around 2030, and the future annual cycles are characterised by an almost constant rise of flow throughout the year. Instead, Greenland rivers present an earlier change to unfamiliar climate by 2027, and a strong intensification of the river discharge peak. It is unlikely a direct impact of such changes in Greenland, Yukon, and

320 Lena on human settlements (like African rivers) as these deltas are mostly depopulated. However, the extra discharge may influence a wide range of physical, chemical, and biological systems (Mankoff et al. 2020 and references therein). For instance, the enhancement of freshwater release may produce a freshening of the Arctic Ocean (Morison et al., 2012), which in turn affects the ocean stratification, the sea ice formation or melt, and potentially the global ocean overturning circulation (Solomon et al., 2021). In agreement with the model simulations, some observation-based studies reported an accelerated rise of Arctic

325 freshwater input from rivers since the 90's favouring the cooling and freshening process (Rabe et al., 2011; Perner et al., 2019; Shiklomanov et al., 2021).

Most rivers in the world present positive flow trends. Two exceptions are Colorado in North America and Limay in the Patagonia, rivers with flows that will remain in the range of natural variability but with a decline of about 15%. The hydrological deficit on these rivers reduces the hydropower generation due to low dams levels, but also reduces the availability of water for

330 irrigation affecting agriculture and livestock. In agreement with our results Hoerling et al. (2019) and Milly and Dunne (2020)

reported a continuous decay of Colorado river flow according to the observations. In the same way, Cerveny et al. (2022) highlighted that nowadays Lake Mead, located behind Hoover Dam, records its lowest level since the 1930s (filled to just 35% of its capacity) threatening the hydroelectric power production of the dam and the provision of water. Similar impacts face communities depending on rivers originating in Southern Andes. Rivera et al. (2021) reported frequent hydrological droughts

335 in the last decade due to the reduced snow accumulation over the the Andes. The continuous low levels of the river systems motivated Argentinian authorities to declare the water emergency for the catchments of Limay, Neuquén, and Negro in 2022, limiting the operation of the dams to guarantee the availability of water in the affected areas.

It is a concern that several important rivers of the world are projected to cross imminently the limit of their natural variability. However, the hydrological predictions presented in this work should be interpreted in the context of a very high baseline emis-

340 sion scenario, i.e., a potential outcome if society does not make concerted efforts to cut greenhouse gas emissions (Van Vuuren et al., 2011). As such, the results may be used as an upper limit for decision making. In future work, we will extend the analysis to a broader set of the new SSP scenarios.

Appendix A: Internal variability in projections of runoff anomaly

345 In our experiments each GCM has only a single ensemble member per resolution and simulation type. It means that the projections may be significantly influenced by internal variability. Deser et al. (2012) tested the internal variability with a set of 40 members of regional climate model simulations of North America and highlighted that projections of precipitation are more subject to internal variability than projections of temperature. Given the direct impact of precipitation on runoff, it could be hypothesized strong internal variability of river flow in model simulations. Such robust internal variability test is

350 not possible in our work given that most GCMs provide a single realization, except by the HadGEM3-GC31 family, which provides three realizations per resolution and simulation type. The realization resulted from varying the initial conditions with a random perturbation to the initial state of the atmosphere. Figure A1a-b exhibits the global runoff anomaly projections of each GCM along with shaded bands representing the internal variability of HadGEM3-GC31 triplets. While the internal variability tend to rise over time, especially in HadGEM3-GC31-LL, it is smaller than the inter-model variability and comparable to the

355 variability given by the GCMs' resolution. Thus, it may be assumed that our set of simulations is adequate for the proposed objectives and that more realizations would not present substantial alter the presented results.

Appendix B: Changes in land precipitation, evapotranspiration, and surface temperature

The IPCC AR6 reports a strengthening of the future global land water budget components with strong regional variations (Douville et al., 2021; Caretta et al., 2022). The results presented in section 3.1 agree with the previous statement at the global
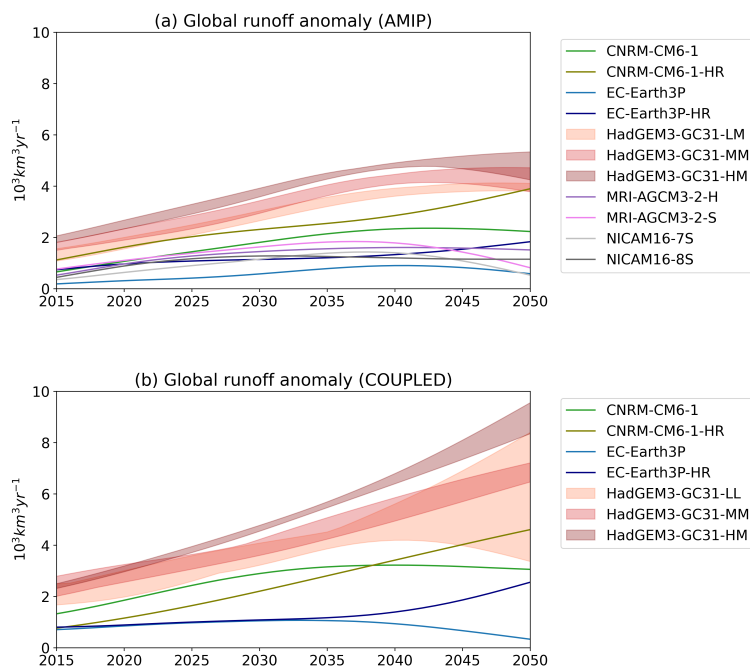
Figure A1. Low-pass filtered projections of global runoff anomalies for (a) AMIP and (b) COUPLED simulations. The solid lines show the projections of individual GCMs. The shaded bands show the internal variability of HadGEM3-GC31 GCM generated by three realizations of the GCM at low-, intermediate-, and high-resolution that vary in the initialization method.

360   scale. Here, we complement those results with focus on the spatial variability of the expected changes in the water cycle. Figure B1a-b complements the Fig. 2 with the maps of the ensemble mean difference between FUTURE and PRESENT for land precipitation and evapotranspiration. These maps present similarities with the runoff map, mainly in the positive changes in the northern high latitudes, the Maritime Continent, and over the Sahel, which dominate the overall intensification of the water cycle.

365   The wetter conditions in the northern high-latitudes observed in Figs. B1a-b are associated with the well-known polar amplification of warming observed in Fig. B1c, however the specific processes responsible for this connection are still a topic of discussion. Some studies explain this relationship in terms of the moisture budget, arguing that either the increased surface evaporation following the retreat of sea ice and glaciers and the thawing of permafrost (Bintanja and Selten, 2014; Kopec et al., 2016) or the stronger moisture advection from lower latitudes (Bengtsson et al., 2011) cause increased precipitation, while

370   Pithan and Jung (2021) support that it is mostly driven by stronger radiative loss of energy to space. Regardless, the rise of precipitation and runoff alter the hydrological dynamic of the rivers flowing in cold regions (Barnett et al., 2005; Wang et al., 2021).

    The wettening in intertropical regions is associated with the strengthening of the ITCZ. According to previous studies, the ITCZ presents a drying tendency at its edges but a strong moistening tendency in its core (Lau and Kim, 2015; Byrne
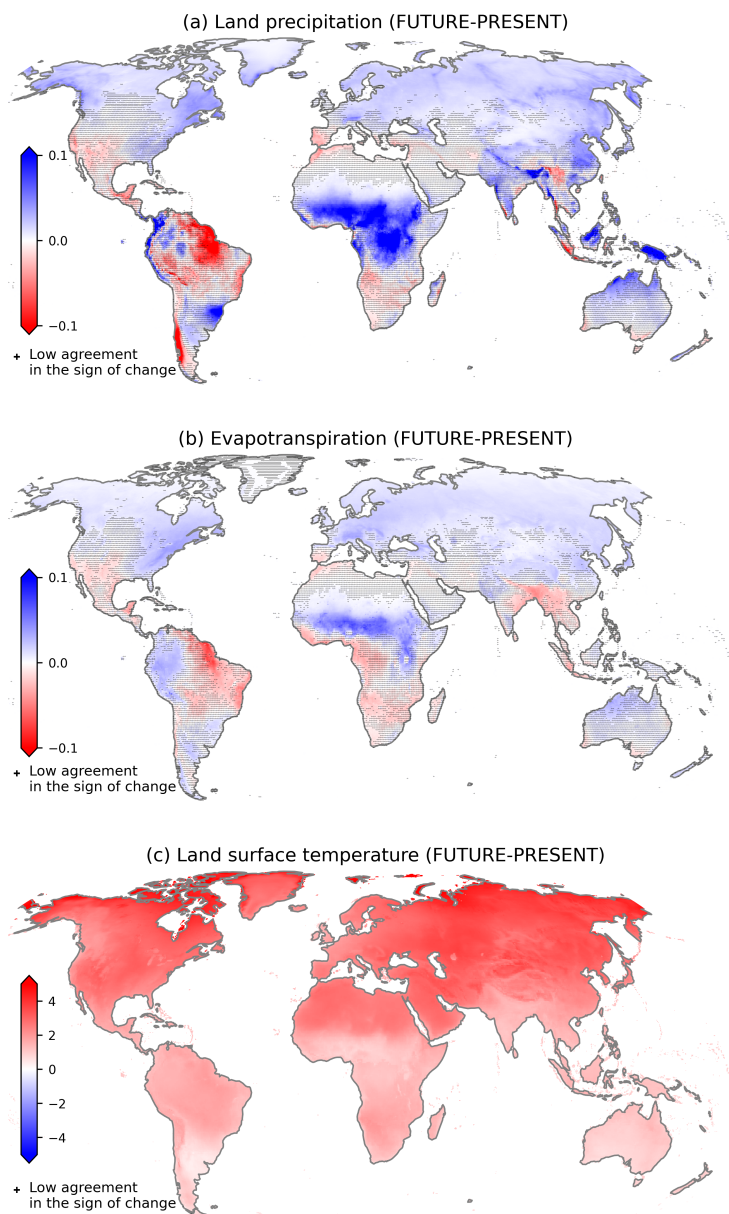
Figure B1. Multi-model ensemble mean differences in (a) land precipitation [10^3km^{3}yr^{-1}], (b) evapotranspiration [10^3km^{3}yr^{-1}], and (c) surface temperature [C] between FUTURE (2015-2050) and PRESENT (1950-2014). The crosses indicate that at least 3 out of 18 GCMs disagree in the sign of change.

375   et al., 2018; Douville et al., 2021). This is attributed to the intensification of ascending motion over the equatorial tropics, which elevates cloud tops, promotes convection processes, and leads to increased intense precipitation (Su et al., 2017). The increased land precipitation is partitioned in extra evapotranspiration and runoff in the Maritime Continent and over the Sahel

(Figs. B1a-b and Fig. 2). However, there are regions presenting some different features. For instance, the Congo basin projects a strong rise of precipitation but combined with a slight evapotranspiration decrease, which favour the strong rise of runoff. This makes it the region of the world with the largest increase in river flow.

Lastly, there are other regions of the world projecting drier conditions of the hydrological cycle that partially compensate its global intensification. For instance, northern Brazil that exhibits reduced precipitation, evapotranspiration, and runoff, or Southern Andes, which shows a strong decay in precipitation combined with enhanced evapotranspiration, which deepens the decrease of runoff and streamflow for the rivers that originate there (see Figs. B1a-b and Fig. 2).

Code and data availability. The HighResMIP CMIP6 GCMs simulations that provide the forcings are freely available on the Earth System Grid Federation (ESGF; esgf-node.llnl.govprojects/cmip6). The standalone river routing code and simulations are stored in JASMIN, the U.K. supercomputer for environmental science deployed on behalf of the Natural Environment Research Council (NERC). They are accessible upon request to the corresponding author.

Author contributions. OVM conceived the research question, performed the simulations, computed and interpreted the results, and wrote the first draft of the paper. PCM, PLV contributed to the conceptualization of the research and the interpretation of the results. EH analyzed and assured the quality of the results given his expertise in ToE methods. All the authors revised the paper and agreed to the submitted version.

Competing interests. The authors declare that they have no conflict of interest.

References

Alkama, R., Decharme, B., Douville, H., and Ribes, A.: Trends in global and basin-scale runoff over the late twentieth century: Methodological issues and sources of uncertainty, J. Climate, 24, 3000–3014, 2011.

400 Alkama, R., Marchand, L., Ribes, A., and Decharme, B.: Detection of global runoff changes: results from observations and CMIP5 experiments, Hydrol. Earth Syst. Sc., 17, 2967–2979, 2013.

Amangabara, G. T. and Obenade, M.: Flood vulnerability assessment of Niger Delta States relative to 2012 flood disaster in Nigeria, American Journal of Environmental Protection, 3, 76–83, 2015.

Barnett, T. P., Adam, J. C., and Lettenmaier, D. P.: Potential impacts of a warming climate on water availability in snow-dominated regions,
405 Nature, 438, 303–309, 2005.

Bengtsson, L., Hodges, K. I., Koumoutsaris, S., Zahn, M., and Keenlyside, N.: The changing atmospheric water cycle in Polar Regions in a warmer climate, Tellus A, 63, 907–920, 2011.

Bintanja, R. and Selten, F.: Future increases in Arctic precipitation linked to local evaporation and sea-ice retreat, Nature, 509, 479–482, 2014.

410 Byrne, M. P., Pendergrass, A. G., Rapp, A. D., and Wodzicki, K. R.: Response of the intertropical convergence zone to climate change: Location, width, and strength, Curr. Clim. Change Rep, 4, 355–370, 2018.

Caretta, M., Mukherji, A., Arfanuzzaman, M., Betts, R., Gelfan, A., Hirabayashi, Y., Lissner, T., Liu, J., Lopez Gunn, E., Morgan, R., Mwanga, S., and Supratid, S.: Water, in: Climate Change 2022: Impacts, Adaptation and Vulnerability. Contribution of Working Group II to the Sixth Assessment Report of the Intergovernmental Panel on Climate Change, edited by Pörtner, H.-O., Roberts, D., Tignor, M.,
415 Poloczanska, E., Mintenbeck, K., Alegría, A., Craig, M., Langsdorf, S., Löschke, S., Möller, V., Okem, A., and Rama, B., chap. 4, pp. 551–712, Cambridge University Press, Cambridge, UK and New York, NY, USA, https://doi.org/10.1017/9781009325844.006, 2022.

Cerveny, N., Balling Jr, R. C., and Cerveny, R.: Dam Weather: The Surprising Impact of Weather on Hoover Dam, Weatherwise, 75, 42–49, 2022.

Chen, M., Shi, W., Xie, P., Silva, V. B., Kousky, V. E., Wayne Higgins, R., and Janowiak, J. E.: Assessing objective techniques for gauge-based
420 analyses of global daily precipitation, Journal of Geophysical Research: Atmospheres, 113, 2008.

Christensen, J. H., Hewitson, B., Busuioc, A., et al.: Regional climate projections. In 'Climate change 2007: the physical science basis. Contribution of Working Group I to the Fourth Assessment Report of the Intergovernmental Panel on Climate Change'.(Eds S Solomon, D Qin, M Manning, Z Chen, M Marquis, KB Averyt, M Tignor, HL Miller) pp. 847–940, 2007.

Clark, E. A., Sheffield, J., van Vliet, M. T. H., Nijssen, B., and Lettenmaier, D. P.: Continental Runoff into the Oceans (1950–2008), J.
425 Hydrometeor., 16, 1502–1520, https://doi.org/10.1175/JHM-D-14-0183.1, 2015.

Conway, D.: Future Nile river flows, Nature Climate Change, 7, 319–320, 2017.

Dai, A., Qian, T., Trenberth, K. E., and Milliman, J. D.: Changes in Continental Freshwater Discharge from 1948 to 2004, J. Climate, 22, 2773–2792, https://doi.org/10.1175/2008JCLI2592.1, 2009.

de Souza Custodio, M., Da Rocha, R. P., Ambrizzi, T., Vidale, P. L., and Demory, M.-E.: Impact of increased horizontal resolution in coupled
430 and atmosphere-only models of the HadGEM1 family upon the climate patterns of South America, Climate Dyn., 48, 3341–3364, 2017.

Decharme, B., Delire, C., Minvielle, M., Colin, J., Vergnes, J.-P., Alias, A., Saint-Martin, D., Séférian, R., Sénési, S., and Voldoire, A.: Recent changes in the ISBA-CTRIP land surface system for use in the CNRM-CM6 climate model and in global off-line hydrological applications, J. Adv. Mod. Earth Sy., 11, 1207–1252, 2019.

Deser, C., Knutti, R., Solomon, S., and Phillips, A. S.: Communication of the role of natural variability in future North American climate,
Nature Climate Change, 2, 775–779, 2012.

Döll, P., Trautmann, T., Gerten, D., Schmied, H. M., Ostberg, S., Saaed, F., and Schleussner, C.-F.: Risks for the global freshwater system at
1.5 C and 2 C global warming, Environmental Research Letters, 13, 044 038, 2018.

Douville, H., Raghavan, K., Renwick, J. Allan, R., Arias, P., Barlow, M., Cerezo-Mota, R., Cherchi, A., Gan, T., Gergis, J., Jiang, D., Khan,
A., Pokam Mba, W., Rosenfeld, D., Tierney, J., and Zolina, O.: Water Cycle Changes, in: Climate Change 2021: Impacts, Adaptation and
Vulnerability. Contribution of Working Group II to the Sixth Assessment Report of the Intergovernmental Panel on Climate Change, edited
by Masson-Delmotte, V., Zhai, P., Pirani, A., Connors, S., Péan, C., Berger, S., Caud, N., Chen, Y., Goldfarb, L., Gomis, M., Huang, M.,
Leitzell, K., Lonnoy, E., Matthews, J., Maycock, T. Waterfield, T., Yelekçi, O., Yu, R., and Zhou, B., chap. 8, pp. 1055–1210, Cambridge
University Press, Cambridge, UK and New York, NY, USA, https://doi.org/10.1017/9781009157896.010, 2021.

Frame, D., Joshi, M., Hawkins, E., Harrington, L. J., and de Roiste, M.: Population-based emergence of unfamiliar climates, Nature Climate
Change, 7, 407–411, 2017.

Gao, H., Bohn, T., Podest, E., McDonald, K., and Lettenmaier, D.: On the causes of the shrinking of Lake Chad, Environmental Research
Letters, 6, 034 021, 2011.

Giorgi, F. and Bi, X.: Time of emergence (TOE) of GHG-forced precipitation change hot-spots, Geophysical Research Letters, 36, 2009.

Gudmundsson, L., Boulange, J., Do, H. X., Gosling, S. N., Grillakis, M. G., Koutroulis, A. G., Leonard, M., Liu, J., Müller Schmied, H.,
Papadimitriou, L., et al.: Globally observed trends in mean and extreme river flow attributed to climate change, Science, 371, 1159–1162,
2021.

Haarsma, R., Roberts, M. J., Vidale, P. L., Senior, C., Bellucci, A., Bao, Q., Chang, P., Corti, S., Fučkar, N. S., Guemas, V., von Hardenberg,
J., Hazeleger, W., Kodama11, C., Koenigk, T., Leung, L. R., Lu, J., Luo, J.-J., Mao, J., Mizielinski, M., Mizuta, R. Nobre, P., Satoh, M.,
Scoccimarro, E., Semmler, T., Small, J., and von Storch, J.-S.: High Resolution Model Intercomparison Project (HighResMIP v1. 0) for
CMIP6, Geosci. Model Dev., 9, 4185–4208, 2016.

Haarsma, R., Acosta, M., Bakhshi, R., Bretonnière, P.-A., Caron, L.-P., Castrillo, M., Corti, S., Davini, P., Exarchou, E., Fabiano, F., , Fladrich,
U., Fuentes Franco, R., García-Serrano, J., von Hardenberg, J., Koenigk, T., Levine, X., Meccia, V. L., van Noije, T., van den Oord, G.,
Palmeiro, F. M., Rodrigo, M., Ruprich-Robert, Y., Le Sager, P., Tourigny, E., Wang, S., van Weele, M., and Wyser, K.: HighResMIP
versions of EC-Earth: EC-Earth3P and EC-Earth3P-HR–description, model computational performance and basic validation, Geoscientific
Model Development, 13, 3507–3527, 2020.

Harrigan, S., Zsoter, E., Alfieri, L., Prudhomme, C., Salamon, P., Wetterhall, F., Barnard, C., Cloke, H., and Pappenberger, F.:
GloFAS-ERA5 operational global river discharge reanalysis 1979–present, Earth System Science Data Discussions, 2020, 1–23,
https://doi.org/10.5194/essd-2019-232, 2020.

Harris, I., Osborn, T. J., Jones, P., and Lister, D.: Version 4 of the CRU TS monthly high-resolution gridded multivariate climate dataset,
Scientific data, 7, 1–18, 2020.

Hawkins, E. and Sutton, R.: Time of emergence of climate signals, Geophysical Research Letters, 39, 2012.

Hawkins, E., Frame, D., Harrington, L., Joshi, M., King, A., Rojas, M., and Sutton, R.: Observed emergence of the climate change signal:
from the familiar to the unknown, Geophysical Research Letters, 47, e2019GL086 259, 2020.

Hersbach, H., Bell, B., Berrisford, P., Hirahara, S., Horányi, A., Muñoz-Sabater, J., Nicolas, J., Peubey, C., Radu, R., Schepers, D., et al.:
The ERA5 global reanalysis, Quart. J. Roy. Meteor. Soc., 2020.

Hoerling, M., Barsugli, J., Livneh, B., Eischeid, J., Quan, X., and Badger, A.: Causes for the century-long decline in Colorado River flow, Journal of Climate, 32, 8181–8203, 2019.

IFRC: Nigeria, Africa | Floods Emergency Appeal (Appeal No: MDRNG034), Tech. rep., International Federation of Red Crosses, https://reliefweb.int/report/nigeria/nigeria-africa-floods-emergency-appeal-appeal-no-mdrng034, 2022.

475 Jung, M., Koirala, S., Weber, U., Ichii, K., Gans, F., Camps-Valls, G., Papale, D., Schwalm, C., Tramontana, G., and Reichstein, M.: The FLUXCOM ensemble of global land-atmosphere energy fluxes, Scientific data, 6, 74, 2019.

Kodama, C., Ohno, T., Seiki, T., Yashiro, H., Noda, A. T., Nakano, M., Yamada, Y., Roh, W., Satoh, M., Nitta, T., Goto, D., Miura, H., Nasuno, T., Miyakawa, T., Chen, Y.-W., and Sugi, M.: The Nonhydrostatic ICosahedral Atmospheric Model for CMIP6 HighResMIP simulations (NICAM16-S): experimental design, model description, and impacts of model updates, Geosci. Model Dev., 14, 795–820, 480 https://doi.org/10.5194/gmd-14-795-2021, 2021.

Koirala, S., Hirabayashi, Y., Mahendran, R., and Kanae, S.: Global assessment of agreement among streamflow projections using CMIP5 model outputs, Environmental Research Letters, 9, 064 017, 2014.

Kopec, B. G., Feng, X., Michel, F. A., and Posmentier, E. S.: Influence of sea ice on Arctic precipitation, Proc. Natl. Acad. Sci. (USA), 113, 46–51, 2016.

485 Lau, W. K. and Kim, K.-M.: Robust Hadley circulation changes and increasing global dryness due to CO2 warming from CMIP5 model projections, Proc. Natl. Acad. Sci. (USA), 112, 3630–3635, 2015.

Lemordant, L. and Gentine, P.: Vegetation response to rising CO2 impacts extreme temperatures, Geophysical Research Letters, 46, 1383–1392, 2019.

Lyu, K., Zhang, X., Church, J. A., Slangen, A., and Hu, J.: Time of emergence for regional sea-level change, Nature Climate Change, 4, 490 1006–1010, 2014.

Mahlstein, I., Knutti, R., Solomon, S., and Portmann, R. W.: Early onset of significant local warming in low latitude countries, Environmental Research Letters, 6, 034 009, 2011.

Mahlstein, I., Portmann, R. W., Daniel, J. S., Solomon, S., and Knutti, R.: Perceptible changes in regional precipitation in a future climate, Geophysical Research Letters, 39, 2012.

495 Mankoff, K. D., Noël, B., Fettweis, X., Ahlstrøm, A. P., Colgan, W., Kondo, K., Langley, K., Sugiyama, S., Van As, D., and Fausto, R. S.: Greenland liquid water discharge from 1958 through 2019, Earth System Science Data, 12, 2811–2841, 2020.

Milly, P. C. and Dunne, K. A.: Colorado River flow dwindles as warming-driven loss of reflective snow energizes evaporation, Science, 367, 1252–1255, 2020.

Mizuta, R., Yoshimura, H., Murakami, H., Matsueda, M., Endo, H., Ose, T., Kamiguchi, K., Hosaka, M., Sugi, M., Yukimoto, S., 500 Kusunoki, S., and Kitoh, A.: Climate Simulations Using MRI-AGCM3.2 with 20-km Grid, J. Meteor. Soc. Japan, Ser II 90A, 233–258, https://doi.org/10.2151/jmsj.2012-A12, 2012.

Mora, C., Frazier, A. G., Longman, R. J., Dacks, R. S., Walton, M. M., Tong, E. J., Sanchez, J. J., Kaiser, L. R., Stender, Y. O., Anderson, J. M., et al.: The projected timing of climate departure from recent variability, Nature, 502, 183–187, 2013.

Morison, J., Kwok, R., Peralta-Ferriz, C., Alkire, M., Rigor, I., Andersen, R., and Steele, M.: Changing arctic ocean freshwater pathways, 505 Nature, 481, 66–70, 2012.

Muelchi, R., Rössler, O., Schwanbeck, J., Weingartner, R., and Martius, O.: River runoff in Switzerland in a changing climate–runoff regime changes and their time of emergence, Hydrology and earth system sciences, 25, 3071–3086, 2021.

Müller, O. V., Vidale, P. L., Vannière, B., Schiemann, R., and McGuire, P. C.: Does the HadGEM3-GC3.1 GCM Overestimate Land Precipitation at High Resolution? A Constraint Based on Observed River Discharge, Journal of Hydrometeorology, 22, 2131 – 2151, https://doi.org/10.1175/JHM-D-20-0290.1, 2021a.

Müller, O. V., Vidale, P. L., Vannière, B., Schiemann, R., Senan, R., Haarsma, R. J., and Jungclaus, J. H.: Land-Atmosphere Coupling Sensitivity to GCMs Resolution: A Multimodel Assessment of Local and Remote Processes in the Sahel Hot Spot, J. Climate, 34, 967–985, https://doi.org/10.1175/JCLI-D-20-0303.1, 2021b.

Nijssen, B., O'Donnell, G. M., Lettenmaier, D. P., Lohmann, D., and Wood, E. F.: Predicting the Discharge of Global Rivers, J. Climate, 14, 3307–3323, https://doi.org/10.1175/1520-0442, 2001.

Obi-Ani, N. A. and Isiani, M. C.: Urbanization in Nigeria: The Onitsha experience, Cities, 104, 102 744, https://doi.org/https://doi.org/10.1016/j.cities.2020.102744, 2020.

Oliver, R. J., Mercado, L. M., Clark, D. B., Huntingford, C., Taylor, C. M., Vidale, P. L., McGuire, P. C., Todt, M., Folwell, S., Shamsudheen Semeena, V., et al.: Improved representation of plant physiology in the JULES-vn5. 6 land surface model: photosynthesis, stomatal conductance and thermal acclimation, Geoscientific Model Development, 15, 5567–5592, 2022.

Perner, K., Moros, M., Otterå, O. H., Blanz, T., Schneider, R. R., and Jansen, E.: An oceanic perspective on Greenland's recent freshwater discharge since 1850, Scientific reports, 9, 1–10, 2019.

Pham-Duc, B., Sylvestre, F., Papa, F., Frappart, F., Bouchez, C., and Crétaux, J.-F.: The Lake Chad hydrology under current climate change, Scientific reports, 10, 1–10, 2020.

Pithan, F. and Jung, T.: Arctic amplification of precipitation changes—The energy hypothesis, Geophys. Res. Lett., 48, e2021GL094 977, 2021.

Rabe, B., Karcher, M., Schauer, U., Toole, J. M., Krishfield, R. A., Pisarev, S., Kauker, F., Gerdes, R., and Kikuchi, T.: An assessment of Arctic Ocean freshwater content changes from the 1990s to the 2006–2008 period, Deep Sea Research Part I: Oceanographic Research Papers, 58, 173–185, 2011.

Ritchie, H. and Roser, M.: Natural Disasters, Our World in Data, https://ourworldindata.org/natural-disasters, 2014.

Rivera, J. A., Otta, S., Lauro, C., and Zazulie, N.: A decade of hydrological drought in Central-Western Argentina, Frontiers in Water, 3, 640 544, 2021.

Rodell, M., Beaudoing, H. K., L'Ecuyer, T., Olson, W. S., Famiglietti, J. S., Houser, P. R., Adler, R., Bosilovich, M. G., Clayson, C. A., Chambers, D., et al.: The observed state of the water cycle in the early twenty-first century, J. Climate, 28, 8289–8318, 2015.

Rudels, B. and Friedrich, H. J.: The transformations of Atlantic water in the Arctic Ocean and their significance for the freshwater budget, in: The freshwater budget of the Arctic Ocean, pp. 503–532, Springer, 2000.

Shiklomanov, A., Déry, S., Tretiakov, M., Yang, D., Magritsky, D., Georgiadi, A., and Tang, W.: River freshwater flux to the Arctic Ocean, in: Arctic hydrology, permafrost and ecosystems, pp. 703–738, Springer, 2021.

Solomon, A., Heuzé, C., Rabe, B., Bacon, S., Bertino, L., Heimbach, P., Inoue, J., Iovino, D., Mottram, R., Zhang, X., et al.: Freshwater in the arctic ocean 2010–2019, Ocean Science, 17, 1081–1102, 2021.

Su, H., Jiang, J. H., Neelin, J. D., Shen, T. J., Zhai, C., Yue, Q., Wang, Z., Huang, L., Choi, Y.-S., Stephens, G. L., et al.: Tightening of tropical ascent and high clouds key to precipitation change in a warmer climate, Nat. Commun., 8, 15 771, 2017.

Trenberth, K. E., Smith, L., Qian, T., Dai, A., and Fasullo, J.: Estimates of the global water budget and its annual cycle using observational and model data, J. Hydrometeor., 8, 758–769, 2007.

545   UNITAR: Situational Update 1: Satellite assessment of floods over the city of N'djamena, Chad, Tech. rep., United Nations Institute for Training And Research, https://unosat.org/products/2151, 2012.

UNOCHA: Republic of Congo: Floods Flash Update N°3, Tech. rep., United Nations Office for the Coordination of Humanitarian Affairs, https://reliefweb.int/report/congo/republic-congo-floods-flash-update-n-3-23-january-2020, 2021.

UNOCHA: Chad : Flooding situation in N'djamena - Situation Report No. 3, Tech. rep., United Nations Office for the Coordination of
550   Humanitarian Affairs, https://reliefweb.int/report/chad/chad-flooding-situation-ndjamena-situation-report-no-03-29102022, 2022.

Van Vuuren, D. P., Edmonds, J., Kainuma, M., Riahi, K., Thomson, A., Hibbard, K., Hurtt, G. C., Kram, T., Krey, V., Lamarque, J.-F., et al.: The representative concentration pathways: an overview, Climatic change, 109, 5–31, 2011.

Vannière, B., Demory, M.-E., Vidale, P. L., Schiemann, R., Roberts, M., Roberts, C., Matsueda, M., Terray, L., Koenigk, T., and Senan, R.: Multi-model evaluation of the sensitivity of the global energy budget and hydrological cycle to resolution, Climate Dyn., 52, 6817–6846,
555   2019.

Vellinga, M., Roberts, M., Vidale, P. L., Mizielinski, M., Demory, M.-E., Schiemann, R., Strachan, J., and Bain, C.: Sahel decadal rainfall variability and the role of model horizontal resolution, Geophys. Res. Lett., 43, 326–333, 2016.

Voldoire, A., Saint-Martin, D., Sénési, S., Decharme, B., Alias, A., Chevallier, M., Colin, J., Guérémy, J.-F., Michou, M., Moine, M.-P., et al.: Evaluation of CMIP6 deck experiments with CNRM-CM6-1, J. Adv. Mod. Earth Sy., 11, 2177–2213, 2019.

560   Wang, J., Kumar Shrestha, N., Aghajani Delavar, M., Worku Meshesha, T., and Bhanja, S. N.: Modelling watershed and river basin processes in cold climate regions: A review, Water, 13, 518, 2021.

Weedon, G. P., Balsamo, G., Bellouin, N., Gomes, S., Best, M. J., and Viterbo, P.: The WFDEI Meteorological Forcing Data, https://doi.org/10.5065/486N-8109, 2018.

Williams, K., Copsey, D., Blockley, E., Bodas-Salcedo, A., Calvert, D., Comer, R., Davis, P., Graham, T., Hewitt, H., Hill, R., Hyder, P.,
565   Ineson, S., Johns, T., Keen, A., Lee, R., Megann, A., Milton, S., Rae, J., Roberts, M., Scaife, A., Schiemann, R., Storkey, D., Thorpe, L., Watterson, I., Walters, D., West, A., Wood, R., Woollings, T., and Xavier, P.: The Met Office Global Coupled Model 3.0 and 3.1 (GC3.0 and GC3.1) Configurations, J. Adv. Mod. Earth Sy., 10, 357–380, https://doi.org/10.1002/2017MS001115, 2018.

Wu, H., Kimball, J. S., Mantua, N., and Stanford, J.: Automated upscaling of river networks for macroscale hydrological modeling, Water Resources Research, 47, 2011.

570   Wu, H., Kimball, J. S., Li, H., Huang, M., Leung, L. R., and Adler, R. F.: A new global river network database for macroscale hydrologic modeling, Water resources research, 48, 2012.